

Neutrino oscillations with atmospheric neutrinos at large liquid argon TPCs

Animesh Chatterjee^{1,2} * and Albert De Roeck¹ †

¹ *European Organization for Nuclear Research (CERN), 1211 Geneva 23, Switzerland and*

² *Physical Research Laboratory, Ahmedabad, Gujarat, 380009, India*

We propose to study atmospheric neutrino interactions with a unique event topology to distinguish neutrinos and anti-neutrinos using a liquid argon time projection chamber in an experiment such as DUNE. The detection of CC1P and CC0P events will allow to access neutrino oscillation physics complementary to accelerator based beam neutrinos. Our analysis shows that a sensitivity to the mass-ordering can be achieved with a significance close to 4σ and a CP violation sensitivity with more than 2σ with a data sample of 140 kt-yr of atmospheric neutrinos in the DUNE detector.

I. INTRODUCTION

Neutrino oscillations, in which one flavour of neutrinos converts into others, have been discovered using a variety of neutrino sources: from neutrinos produced in the sun to atmospheric neutrinos, from reactors to accelerators, and with a variety of detection techniques in different terrestrial experiments[1, 2].

Atmospheric neutrinos have played a key role in discovering and understanding neutrino oscillations [3]. The first hint of resilient signatures of deviations from the Standard Model in neutrinos came from a deficit of muon neutrinos in IMB [4] and Kamiokande [5], which was later firmly established by the Super-Kamiokande (SuperK)[6] experiment.

In the last two decades, the neutrino community has developed a vast program using accelerator, reactor, and solar neutrinos to measure the oscillation patterns. The future long-baseline facility Deep Underground Neutrino Experiment (DUNE)[7] aims to extract the sign of the atmospheric mass splitting and the CP-violating phase δ_{CP} through the golden channels $\nu_\mu \rightarrow \nu_e$ and $\bar{\nu}_\mu \rightarrow \bar{\nu}_e$. However, both quantities can also be extracted using atmospheric neutrinos as proposed in the literature since a long time[8–12].

The oscillation phenomenology of atmospheric neutrinos is exceptionally rich because it covers 10 orders of magnitude in the ratio of baseline distance to the energy, (L/E_ν). The baseline L covers the range from 15 to 12700 km and the neutrino energy ranges from $\mathcal{O}(10^{-2})$ to $\mathcal{O}(10^5)$ GeV. This broad (L/E_ν) spectrum and the large matter effects induced by the Earth's matter density profile lead to non-trivial oscillation effects, namely MSW [13, 14] and parametric [15] matter resonances. In this letter we are particularly interested in studying the rich oscillation phenomenology of the wide energy region; from sub-GeV (<1 GeV) to 10s of GeV atmospheric neutrinos. The primary reasons are the following. First, the oscillation of sub-GeV neutrinos with a large baseline (Earth radius) is strongly affected by both solar and atmospheric mass splittings.

The effects on oscillation probabilities of the leptonic CP violating phase δ_{CP} are much more pronounced in sub-GeV atmospheric neutrinos compared to long-baseline accelerator-based beam neutrinos[16]. Hence, a measurement of the oscillation pattern with the wide energy range (from sub-GeV to 10s of GeV) can provide important new information on the measurement of δ_{CP} . Second, the broad energy spectrum and large matter effects induced by the Earth's matter density profile lead to non-trivial oscillation effects that will help to resolve mass ordering[17, 18]. Third, the pioneering technique of liquid argon time projection chambers (LArTPCs)[19] allows for excellent reconstruction of neutrino event topologies. This unique technique will help to separate neutrino and anti-neutrino samples coming from atmospheric neutrinos, as discussed below. Therefore, such measurements will not only have a significant impact on the CP violation but also on resolving the mass ordering and octant degeneracy.

Motivated by the previous study on the CP violation using sub-GeV atmospheric neutrinos at DUNE[16], in this Letter, we propose to study the atmospheric neutrinos (with a wide range of energies from 100 MeV to 10 GeV), using unique event topology to distinguish neutrinos and anti-neutrinos using the liquid argon time projection chamber at DUNE as an example to measure the neutrino oscillation effects. Such measurements can be likely conducted to a significant part already before beam data taking starts with its full power, in the present anticipated sequencing schedule of that experiment.

II. NEUTRINO OSCILLATIONS WITH ATMOSPHERIC NEUTRINOS

In the three neutrino oscillation scenario, neutrino oscillations are described by six parameters : three mixing angles ($\theta_{12}, \theta_{13}, \theta_{23}$), two mass-squared differences ($\Delta m_{21}^2, \Delta m_{31}^2$) and a complex phase that parametrizes the violation of the CP symmetry (δ_{CP}) in the lepton sector[20, 21]. Currently, the unknowns in the standard oscillation sector are the mass ordering among the three neutrino states, the octant of the atmospheric mixing angle θ_{23} , and the value of the CP violating phase δ_{CP} .

* animesh@cern.ch

† Albert.de.Roeck@cern.ch

When neutrinos travel through matter their coherent forward charged current scattering off the ambient electrons leads to an extra effective contribution to the neutrino mass matrix. In atmospheric neutrino oscillations, generally the dominant mixing angle is θ_{23} , and the relevant mass-squared difference is Δm_{31}^2 . However, in the sub-GeV region, and for baselines of approximately 1000 km, the neutrino evolution is dominated by Δm_{21}^2 . The finite energy resolution makes the experiments inaccessible to the oscillation driven by Δm_{31}^2 and Δm_{32}^2 . We discuss the oscillation phenomenology for the wide energy range and baseline length below.

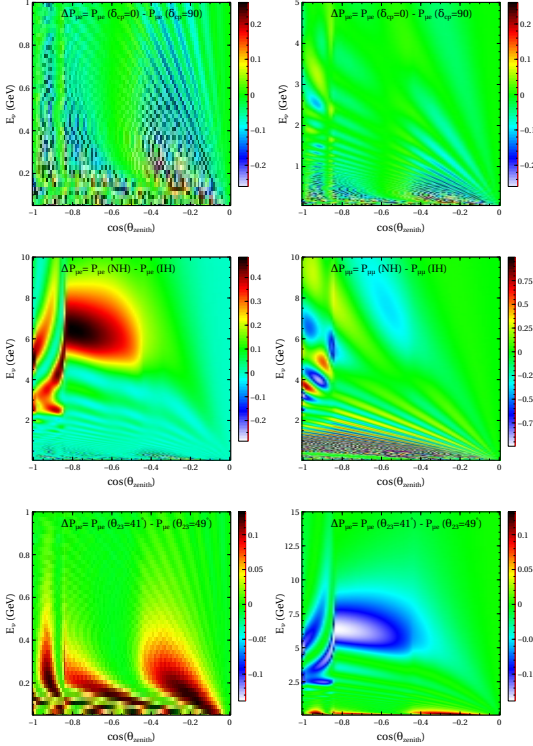


FIG. 1. Top: Difference of the muon-appearance probability for a CP conserving ($\delta_{cp} = 0$) and a CP violating ($\delta_{cp} = 90^\circ$) phase is shown both for sub-GeV (left) and high energy (right) region as a function of the neutrino energy and cosine of the zenith angle. Middle: Difference of the muon-appearance probability (left) and muon-disappearance probability (right) for the two different mass-orderings is shown both as a function of neutrino energy and cosine of the zenith angle. Bottom: Difference of the muon-appearance probability for lower octant ($\theta_{23} = 41^\circ$) and higher octant ($\theta_{23} = 49^\circ$) is shown both for the sub-GeV (left) and high energy (right) region as function of the neutrino energy and cosine of the zenith angle.

First we discuss the effects of δ_{CP} in the oscillation of atmospheric neutrinos. The CP violating term in the oscillation probability can be written as [22]

$$\Delta_{CP} = -8J_r \sin(\delta_{cp}) \sin(\Delta_{12}) \sin(\Delta_{23}) \sin(\Delta_{13}) \quad (1)$$

where $\Delta_{ij} = \delta m_{ij}^2 L / 4E$ and $J_r = c_{12}s_{12}c_{23}s_{23}c_{13}^2s_{13}^2$, where $c_{ij} = \cos \theta_{ij}$ and $s_{ij} = \sin \theta_{ij}$ respectively. To

understand the δ_{cp} effects, we need to separate the atmospheric neutrinos in two different energy region; i) E_ν sub-GeV: in this energy range, oscillations of atmospheric neutrinos are governed by both the atmospheric mass splitting Δm_{31}^2 and by Δm_{21}^2 . In this energy range, the oscillations driven by Δm_{31}^2 are fast and average out, leading to a much larger CP-violating term compared to beam neutrino studies. The top left panel of Fig. 1 shows the difference of the electron appearance channel probability for $\delta_{cp} = 0$ and $\pi/2$ values. This clearly shows that the sub-GeV energy region will provide significant sensitivity to CP violation from atmospheric neutrinos. ii) $E_\nu > 1$ GeV: in this energy range the oscillations are mostly dominated by the atmospheric mass splitting. Hence, the CP term will be suppressed by a factor of $\Delta m_{21}^2 / \Delta m_{31}^2 * \pi/2 \approx 1/25$ [23] as can be seen from the top right plot of Fig. 1.

To describe the mass-ordering and octant sensitivity arising from atmospheric neutrinos, we use the appearance probability [24, 25], which is valid for a constant matter density, and given by

$$\begin{aligned} P_{\mu e} \approx & 4 \sin^2 \theta_{13} \sin^2 \theta_{23} \frac{\sin^2 \Delta_{31} (1 - f mA)}{(1 - f mA)^2} \\ & + m * \frac{\Delta m_{21}^2}{\Delta m_{31}^2} \sin 2\theta_{13} \sin 2\theta_{12} \sin 2\theta_{23} \\ & * \cos(m\Delta_{31} + f\delta_{cp}) \frac{\sin \Delta_{31} A}{A} \frac{\sin \Delta_{31} (1 - f mA)}{(1 - f mA)} \end{aligned} \quad (2)$$

where $f = 1$ for neutrinos and $f = -1$ for anti-neutrinos, $m = \text{sign}(\Delta m_{31}^2)$. The matter effect comes into play via the term $A = 2EV / \Delta m_{31}^2$, where V is the matter potential. The dependence of the appearance channel on the mass-ordering is proportional to the matter effect. Hence, large matter effects with a wide energy range of atmospheric neutrinos will have a significant impact in resolving the mass-ordering. The difference of the two mass ordering schemes for $P_{\mu e}$ (left) and $P_{\mu\mu}$ (right) as a function of energy and cosine of the zenith angle is shown in the middle panel of Fig. 1. The oscillogram plots clearly demonstrate that large matter effects plays a crucial role in the appearance channel across the wide neutrino energy range. Hence, a mass-ordering sensitivity arises both in the muon and electron channel from atmospheric neutrinos.

The ν_e appearance also depends on $\sin^2 \theta_{23}$ leading to the possibility to resolve the octant of θ_{23} degeneracy. Hence, the possibility of detecting atmospheric neutrinos and antineutrinos with a LArTPC detector such as DUNE enables these experiments to resolve differences in the oscillation of both modes. The difference of muon-appearance probability for lower octant ($\theta_{23} = 41^\circ$) and higher octant ($\theta_{23} = 49^\circ$) is shown both for the sub-GeV (left) and high energy (right) region as a function of cosine of zenith angle in the bottom panel of Fig. 1. It is apparent that the sub-GeV atmospheric data will also help to resolve the octant degeneracy.

III. NEUTRINO INTERACTIONS AND EVENT TOPOLOGY WITHIN LARTPC DETECTOR

Atmospheric neutrinos cover a wide range of energies in which neutrinos may interact via the exchange of charged or neutral currents. The relevance of distinct interaction channels differs from one experiment to another, since they measure the atmospheric flux at different energy scales. Therefore, we need to evaluate the different interaction channels as they may affect the determination of oscillation parameters in a different way in each experiment.

Charged-current neutrino interactions can be classified in three major different types: a) Charged current quasielastic (CCQE) : these interactions dominate in the lower-energy region, below 2 GeV, and scatter off one of the bound nucleons, emitting the charged-lepton partner of the interacting neutrino. The outgoing nucleon is either a proton, for neutrinos, or a neutron, for antineutrinos. These interactions are most relevant in the sub-GeV region of the energy spectrum. b) Resonance production (CCRES): at slightly higher energies up to 4 GeV, neutrinos can excite an entire nucleon, producing a baryon resonance that, in turn, quickly decays into a nucleon and a single or multiple mesons. Similar to CCQE, in these interactions, antineutrinos tend to produce more neutrons than protons in the final state. c) Deep inelastic scattering (CC DIS): at energies above 4 GeV, neutrinos can scatter off a single quark inside the nucleon, producing the corresponding charged lepton plus a hadronic shower in the final state. In this type of event, the flavor reconstruction may get confused unless the outgoing charged lepton has sufficient momentum to be distinguished from the hadronic showers. For this first analysis we will use only neutrinos with energies below 10 GeV, and explore the charge identification potential in the region of neutrinos with energies < 4 GeV.

At present, Super-Kamiokande and IceCube are the only large Cherenkov detectors recording atmospheric neutrinos. But explicit measurement of sub-GeV neutrinos is lacking. The major difficulty in detecting these neutrinos is due to the limited event reconstruction capabilities, which is very challenging for these experiments at these low energies. When a sub-GeV neutrino scatters on a nucleon via CCQE interactions, it produces a charged lepton and a proton, for neutrinos, or a neutron, for antineutrinos respectively. Protons with less than 1.4 GeV do not emit any Cherenkov light in water, and hence can not be used to distinguish between neutrino and antineutrinos.

The Liquid Argon Time Projection Chamber (LARTPC) with its full 3D-imaging, excellent particle identification (PID) capability and precise calorimetric energy reconstruction represents the most advanced experimental technology for neutrino detection for large detectors. Recently the ArgoNeut experiment [26, 27] has shown that protons with kinetic energy above 21 MeV can be efficiently identified. It has also shown that the detec-

tion of these protons allows the separation between sub-GeV neutrino and anti-neutrino interactions with Argon. Hence, together with the excellent energy resolution and identification of low energy proton, LARTPC detectors will be able to separate neutrino (CC1P) and anti-neutrino (CC0P) events distinctively below 4 GeV at DUNE[28–30].

IV. EXPERIMENTAL DETAILS

The atmospheric neutrino and anti-neutrino events are obtained by folding the relevant incident fluxes with the appropriate disappearance and appearance probabilities, charge current (CC) cross sections, detector efficiency, resolution, detector mass, and exposure time. The μ^- , and e^- event rates in an energy bin of width dE_ν and in a solid angle bin of width $d\Omega_\nu$ are as follows:

$$\frac{d^2 N_\mu}{d\Omega dE} = \frac{D_{\text{eff}} \Sigma}{2\pi} \left[\left(\frac{d^2 \Phi_\mu}{d \cos \theta dE} \right) P_{\mu\mu} + \left(\frac{d^2 \Phi_e}{d \cos \theta dE} \right) P_{e\mu} \right]. \quad (3)$$

$$\frac{d^2 N_e}{d\Omega dE} = \frac{D_{\text{eff}} \Sigma}{2\pi} \left[\left(\frac{d^2 \Phi_\mu}{d \cos \theta dE} \right) P_{\mu e} + \left(\frac{d^2 \Phi_e}{d \cos \theta dE} \right) P_{ee} \right] \quad (4)$$

Here Φ_μ and Φ_e are the ν_μ and ν_e atmospheric fluxes respectively, obtained from Honda et al.[31, 32] at the Homestake site; $P_{\mu\mu}$ (P_{ee}) and $P_{\mu e}$ are disappearance and appearance probabilities; Σ is the total charge current (CC) cross-section taken from GENIE MC generator [33] and D_{eff} is the detector efficiency. The μ^+ , and e^+ event rates are similar to the above expression with the fluxes, probabilities, and cross sections replaced by those for $\bar{\nu}_\mu$ and $\bar{\nu}_e$ respectively. For a LARTPC detector, the energy and angular resolution are implemented using a Gaussian resolution function as follows,

$$R_{E_\nu}(E_t, E_m) = \frac{1}{\sqrt{2\pi}\sigma} \exp \left[-\frac{(E_m - E_t)^2}{2\sigma^2} \right]. \quad (5)$$

$$R_{\theta_\nu}(\Omega_t, \Omega_m) = N \exp \left[-\frac{(\theta_t - \theta_m)^2 + \sin^2 \theta_t (\phi_t - \phi_m)^2}{2(\Delta\theta)^2} \right], \quad (6)$$

where N is a normalization constant. Here, E_m (Ω_m), and E_t (Ω_t) denote the measured and true values of energy (zenith angle) respectively. The smearing width σ is a function of the energy E_t . Assumptions of the experimental smearing for the DUNE Far Detector (LARTPC) parameters for this study are reported in Table I and taken from [34–36].

Parameter uncertainties or values	Value
$\mu^{+/-}$ angular uncertainty	3°
$e^{+/-}$ angular uncertainty	5°
proton angular uncertainty	10°
$\mu^{+/-}$ energy uncertainty	3%
$e^{+/-}$ energy uncertainty	5%
proton energy uncertainty	10%
Detection efficiency	85%
Charge mis-identification efficiency	5%
Flux normalization	10%
Zenith angle uncertainty	25°
Cross section uncertainty	20%
Additional overall systematic	5%
Flux Tilt[10]	5%

TABLE I. Assumptions of the LArTPC Far Detector parameters and uncertainties.

Neutrino (anti-neutrino) events in the LArTPC detector are classified by event topology. We consider neutrino (anti-neutrino) events with a charged lepton (muon or electron) and 1 outgoing proton; for neutrinos the topology is used is CC1P and CC0P for anti-neutrinos. This technique is applied up to a neutrino energy of 4 GeV. The threshold kinetic energy for proton identification within LArTPC can be as low as 21 MeV as shown in [26], but in our analysis we have used a more conservative energy threshold of 30 MeV. In this analysis neutrino energy reconstructed as $E_\nu = E_{lepton} + K_{proton}$, where K_{proton} is the proton kinetic energy. Any neutrino event with proton energy higher than 30 MeV is included in this analysis. Neutrino and anti-neutrino events are summed (for the same flavour) for each energy and angular bins above 4 GeV. We show the CC1P event distribution with true input value $\delta_{cp} = \pi/2$ (left) and the difference of CC1P events with $\delta_{cp} = 0$ (right) as a function of neutrino energy (sub-GeV region) and $\cos(\theta_{zenith})$ for 140 kt-yr (see table II) of atmospheric data in Fig. 2. The right panel of Fig. 2 shows that there are a total of 40 bins, which will provide significant sensitivity to the CP violation from sub-GeV energy region.

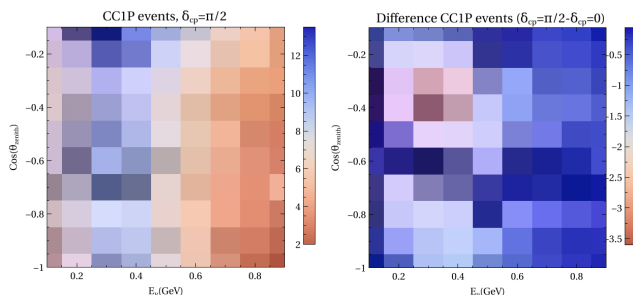


FIG. 2. CC1P event distribution with true input value $\delta_{cp} = \pi/2$ (left) and the difference of CC1P events with $\delta_{cp} = 0$ (right) as a function of neutrino energy (sub-GeV region) and $\cos(\theta_{zenith})$ for 140 kt-yr of atmospheric data only.

V. ANALYSIS AND RESULTS

The computation of χ^2 is performed using the method of pulls. This method allows us to take into account the various statistical and systematic uncertainties in a straightforward way. The flux, cross sections and other systematic uncertainties are included by allowing these inputs to deviate from their standard values in the computation of the expected rate in the i - j^{th} bin, N_{ij}^{th} .

$$N_{ij}^{\text{th}} = N_{ij}^{\text{th}}(\text{std}) + \sum_{k=1}^{\text{npull}} \sigma_{ij}^k \xi_k, \quad (7)$$

where $N_{ij}^{\text{th}}(\text{std})$ is the expected rate in the i - j^{th} bin calculated with the standard values of the inputs. σ_{ij}^k and ξ_k are the values of the uncertainties and the pull respectively. The χ^2 is calculated as described in [37], which includes the effects of all theoretical and systematic uncertainties (as reported in Table I). In the case of the DUNE LArTPC detector, the χ^2 with charge-id below 4 GeV neutrino energy is calculated as follows,

$$\chi_{<4\text{GeV}}^2 = \chi_{\mu^-}^2 + \chi_{\mu^+}^2 + \chi_{e^-}^2 + \chi_{e^+}^2 \quad (8)$$

and χ^2 without charge-id above 4 GeV neutrino energy

$$\chi_{>4\text{GeV}}^2 = \chi_{\mu^- + \mu^+}^2 + \chi_{e^- + e^+}^2 \quad (9)$$

Finally, $\Delta\chi^2$ is marginalized over the oscillation parameters, given in Table III[38]. To calculate the experimental sensitivity, we have simulated events for up-going atmospheric neutrinos ($\cos(\theta_{zenith}) \simeq -1$). The assumptions on the collected data samples per year are given in Table II. Note that this is an optimistic scenario where, following the installation of the first Far Detector, each year another detector, up to four in total, is assumed to be added and leads to a data collection of 140 kt-year in five years. Presently, the Far Detectors three and four are likely to become ready somewhat later, so the first 5 years will collect perhaps more closer to 100 kt-year. But in any case the atmospheric neutrino program is expected to start several years earlier than the neutrino beam program.

Year	kt-year	Parameters	True Values	Range
First	10	θ_{12}	33.47°	N.A.
Second	20	θ_{13}	8.54°	N.A.
Third	30	θ_{23}	45°	41°: 49°
Fourth	40	Δ_{21}	$7.42 \times 10^{-5} \text{ eV}^2$	N.A.
Fifth	40	Δ_{31}	$2.515 \times 10^{-3} \text{ eV}^2$	$(2.41 - 2.61)10^{-3}$
Total	140	δ_{cp}	0	-180°: 180°

Table II

Table III

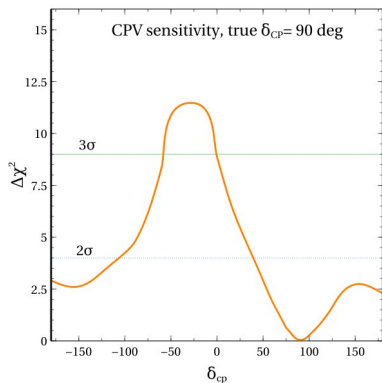


FIG. 3. Sensitivity to the CP violating phase δ_{CP} using atmospheric neutrinos for true $\delta_{CP} = 90^\circ$ with an exposure of 140 kt-yr the DUNE LArTPC detector data.

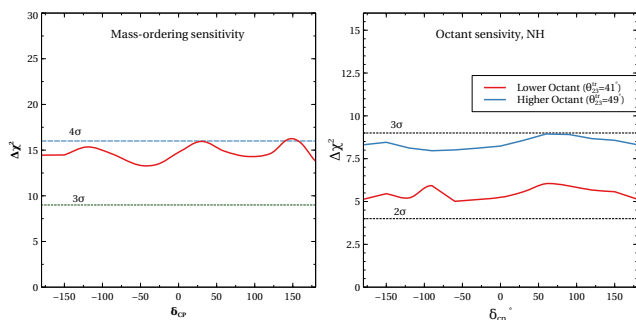


FIG. 4. Sensitivity to the mass-ordering (left) and octant of θ_{23} (right) using atmospheric neutrinos with an exposure of 140 kt-yr of LArTPC detector data such as DUNE.

The sensitivity to the CP violating phase δ_{CP} using only atmospheric neutrinos for true $\delta_{CP} = 90^\circ$ with an exposure of 140 kt-yr of LArTPC data at DUNE is shown in Fig. 3. The result shows that a large region of δ_{CP} parameter space can be excluded with more than 2σ and a fraction of δ_{CP} space with more than 3σ with 140 kt-yr (≈ 5 years) of atmospheric data only. The sensitivity to the CPV can be understood as follows: as discussed before, the CP violation effect for sub-GeV atmospheric neutrinos is a sizable effect, an order of magnitude larger than the corresponding sensitivity for the expected GeV-level beam neutrinos. The best way to measure the CP sensitivity is to separately measure oscillations of the neutrino and anti-neutrino with $\nu_\mu \rightarrow \nu_e$ and $\bar{\nu}_e \rightarrow \bar{\nu}_\mu$ (and charge conjugated). The lower cherenkov threshold for protons inside a LArTPC detector provides the opportunity to distinguish neutrino and anti-neutrino sample by using the event topology inside the LArTPC. For low energies (< 4 GeV), a neutrino interaction is more likely to kick out a proton from a nucleus than an antineutrino interaction, and vice-versa for neutrons. hence, the CC1P sample is neutrino rich while CC0P is antineutrino rich. The combination of these two factors drive the CPV the sensitivity at DUNE.

In Fig. 4, the sensitivity to the mass-ordering (left) and

octant of θ_{23} (right) is shown using atmospheric neutrinos with an exposure of 140 kt-yr for DUNE. A significant sensitivity to the mass ordering may be achieved for all δ_{CP} values with a sensitivity close to 4σ . The reason behind this very promising result is twofold. First, the large matter effect due to the long baseline enhances the sensitivity for all energies as shown in the middle panel of Fig. 1. Second, the separation of neutrinos and anti-neutrinos within a LArTPC provides significant sensitivity to the mass-ordering within the energy range 1-4 GeV. Also notice that, in the case of normal ordering, the matter resonance effects are at the aforementioned energies (2–8 GeV) for almost vertical upgoing neutrinos, $-1 < \cos(\theta_{zenith}) < -0.5$, while for the inverted ordering, such a resonant enhancement in the transition probabilities will take place in the antineutrino channel instead. Hence, the combination of both large matter effect and charge separation helps to get a strong sensitivity to the mass-ordering. The sensitivity to the octant of θ_{23} for the higher (blue) and lower (red) octant is shown in right panel of Fig. 4. The sensitivity of the higher and lower octant are to a level of 3σ and larger than 2σ , respectively. The octant sensitivity mostly arises from appearance channel, $\nu_\mu \rightarrow \nu_e$ and $\bar{\nu}_e \rightarrow \bar{\nu}_\mu$ for atmospheric neutrinos across the wide energy range as can be seen from bottom panel of Fig. 1.

As a next step one could study the impact of using such atmospheric neutrino data with the data from the early neutrino beam, when these become available a few years after the completion of the first Far Detector. In addition, one can try to extend the atmospheric neutrino analysis for the higher energy data (> 4 GeV) including statistical methods for the charge determination, which we intend to study in detail in a forthcoming publication. However, it is clear that atmospheric neutrinos will allow for a pioneering data-driven analysis of both CP violation, mass-ordering and octant determination of θ_{23} using the wide energy range of atmospheric neutrinos in the initial data taking period of DUNE, when fully exploring the unique capabilities of liquid argon time projection chambers.

VI. CONCLUSIONS

Large LArTPCs are becoming available for the study of neutrino physics, and these detectors have excellent capabilities to reconstruct and classify neutrino interactions by topology, which give a sensitivity to neutrino and anti-neutrino interactions. This can be used to study neutrino oscillations and extract the CP violation, neutrino mass ordering and the octant determination of θ_{23} parameters. The results show that with a data sample collected over several years, one can achieve interesting sensitivities to these quantities, complementary to first neutrino beam results. These measurements can however start when the the first Far Detector of the DUNE experiment is completed and starts collecting data.

ACKNOWLEDGMENTS

AC acknowledges CERN Neutrino Platform and the Ramanujan Fellowship (RJF/2021/000157), of the Sci-

ence and Engineering Research Board of the Department of Science and Technology, Government of India. ADR acknowledges CERN Neutrino platform. It is to be noted that this work has been done solely by the authors and is not representative of the DUNE collaboration.

-
- [1] A. B. McDonald, *Rev. Mod. Phys.* **88**, 030502 (2016).
 [2] T. Kajita, *Rev. Mod. Phys.* **88**, 030501 (2016).
 [3] P. Lipari, in *International Conference on History of the Neutrino: 1930-2018* (2018).
 [4] R. Becker-Szendy *et al.*, *Phys. Rev. Lett.* **69**, 1010 (1992).
 [5] K. S. Hirata *et al.* (Kamiokande-II), *Phys. Lett. B* **280**, 146 (1992).
 [6] Y. Ashie *et al.* (Super-Kamiokande), *Phys. Rev. Lett.* **93**, 101801 (2004), arXiv:hep-ex/0404034.
 [7] B. Abi *et al.* (DUNE), (2020), arXiv:2002.03005 [hep-ex].
 [8] M. C. Banuls, G. Barenboim, and J. Bernabeu, *Phys. Lett. B* **513**, 391 (2001), arXiv:hep-ph/0102184.
 [9] R. Gandhi, P. Ghoshal, S. Goswami, P. Mehta, S. U. Sankar, and S. Shalgar, *Phys. Rev. D* **76**, 073012 (2007), arXiv:0707.1723 [hep-ph].
 [10] M. C. Gonzalez-Garcia and M. Maltoni, *Phys. Rev. D* **70**, 033010 (2004), arXiv:hep-ph/0404085.
 [11] S. Choubey, *Nucl. Phys. B Proc. Suppl.* **221**, 46 (2011), arXiv:hep-ph/0609182.
 [12] C. A. Argüelles, P. Fernández, I. Martínez-Soler, and M. Jin, *Phys. Rev. X* **13**, 041055 (2023), arXiv:2211.02666 [hep-ph].
 [13] L. Wolfenstein, *Phys. Rev. D* **17**, 2369 (1978).
 [14] S. P. Mikheyev and A. Y. Smirnov, *Sov. J. Nucl. Phys.* **42**, 913 (1985).
 [15] E. K. Akhmedov, *Sov. J. Nucl. Phys.* **47**, 301 (1988).
 [16] K. J. Kelly, P. A. Machado, I. Martinez Soler, S. J. Parke, and Y. F. Perez Gonzalez, *Phys. Rev. Lett.* **123**, 081801 (2019), arXiv:1904.02751 [hep-ph].
 [17] R. Gandhi, P. Ghoshal, S. Goswami, and S. U. Sankar, *Phys. Rev. D* **78**, 073001 (2008), arXiv:0807.2759 [hep-ph].
 [18] V. Barger, R. Gandhi, P. Ghoshal, S. Goswami, D. Marfatia, S. Prakash, S. K. Raut, and S. U. Sankar, *Phys. Rev. Lett.* **109**, 091801 (2012), arXiv:1203.6012 [hep-ph].
 [19] C. Rubbia, (1977).
 [20] F. Capozzi, E. Di Valentino, E. Lisi, A. Marrone, A. Melchiorri, and A. Palazzo, *Phys. Rev. D* **95**, 096014 (2017), [Addendum: *Phys.Rev.D* 101, 116013 (2020)], arXiv:2003.08511 [hep-ph].
 [21] F. Capozzi, E. Lisi, A. Marrone, D. Montanino, and A. Palazzo, *Nucl. Phys. B* **908**, 218 (2016), arXiv:1601.07777 [hep-ph].
 [22] P. B. Denton, H. Minakata, and S. J. Parke, *JHEP* **06**, 051 (2016), arXiv:1604.08167 [hep-ph].
 [23] O. L. G. Peres and A. Y. Smirnov, *Phys. Lett. B* **456**, 204 (1999), arXiv:hep-ph/9902312.
 [24] J. Elefant and T. Schwetz, *JHEP* **09**, 016 (2015), arXiv:1506.07685 [hep-ph].
 [25] M. Freund, *Phys. Rev. D* **64**, 053003 (2001).
 [26] O. Palamara (ArgoNeuT), *JPS Conf. Proc.* **12**, 010017 (2016).
 [27] R. Acciarri *et al.* (ArgoNeuT), *Phys. Rev. D* **99**, 012002 (2019), arXiv:1810.06502 [hep-ex].
 [28] C. Andreopoulos, C. Barry, S. Dytman, H. Gallagher, T. Golan, R. Hatcher, G. Perdue, and J. Yarba, (2015), arXiv:1510.05494 [hep-ph].
 [29] P. e. Abratenko (MicroBooNE Collaboration), *Phys. Rev. D* **102**, 112013 (2020).
 [30] P. e. Abratenko (MicroBooNE Collaboration), *Phys. Rev. Lett.* **123**, 131801 (2019).
 [31] M. Honda, M. S. Athar, T. Kajita, K. Kasahara, and S. Midorikawa, .
 [32] M. Honda, M. Sajjad Athar, T. Kajita, K. Kasahara, and S. Midorikawa, *Phys. Rev. D* **92**, 023004 (2015), arXiv:1502.03916 [astro-ph.HE].
 [33] C. Andreopoulos *et al.*, *Nucl. Instrum. Meth. A* **614**, 87 (2010), arXiv:0905.2517 [hep-ph].
 [34] T. Alion *et al.* (DUNE), (2016), arXiv:1606.09550 [physics.ins-det].
 [35] B. Abi *et al.* (DUNE), (2018), arXiv:1807.10334 [physics.ins-det].
 [36] G. D. Barr, T. K. Gaisser, S. Robbins, and T. Stanev, *Phys. Rev. D* **74**, 094009 (2006), arXiv:astro-ph/0611266.
 [37] A. Chatterjee, P. Mehta, D. Choudhury, and R. Gandhi, *Phys. Rev. D* **93**, 093017 (2016), arXiv:1409.8472 [hep-ph].
 [38] S. Gariazzo, C. Giunti, M. Laveder, and Y. F. Li, *JHEP* **06**, 135 (2017), arXiv:1703.00860 [hep-ph].